ELSEVIER

Journal of Nuclear Materials 248 (1997) 275–280

journal of nuclear materials

BWR Zircaloy cladding corrosion behavior – effect of microstructure

S. Shimada *, Y. Etoh, K. Tomida

Nippon Nuclear Fuel Development Co., Ltd., 2163, Narita-cho, Oarai-machi, Higashi-ibaraki-gun, Ibaraki-ken 311-13, Japan

Abstract

Corrosion behavior of three types of cladding tubes used in commercial boiling water reactors was evaluated in terms of its correlation to their original second phase particle (SPP) sizes. The mean particle sizes ranged from about 0.07 to 0.4 μm and the maximum fuel burnup was about 46 GW d/t. The results showed that nodular corrosion tended to disappear and the maximum oxide thickness decreased with decreasing particle size. The results also suggested that the SPP size of the current Zircaloy-2 cladding tube used in Japan was in the most preferable range. The effect of temperature on the dissolution of the particles was discussed, and it was pointed out that the variation of temperature experienced by cladding tubes in light water reactors had a significant effect on the dissolution phenomenon. © 1997 Elsevier Science B.V.

1. Introduction

Water-side corrosion of fuel cladding is a potential factor limiting fuel rod performance. In boiling water reactors (BWRs), Zircaloy-2 has been used for the cladding of the fuel rods, and a localized form of corrosion, called nodular oxide, was commonly found on early Zircaloy-2 tubes. Although the whitish nodular oxide is normally thicker than the black oxide widely observed on oxidized Zircaloy, and its appearance is unfavorable, its presence does not cause any problems under most operating conditions. Recent studies [1,2] have shown that the nodular corrosion resistance of Zircaloy-2 could be correlated to the size and distribution of the second-phase particles (SPPs) or precipitates, which could be controlled by heat treatment conditions during the fabrication process. The results also indicated that an increased nodular corrosion resistance of Zircaloy-2 correlated to increasing precipitate number density or decreasing particle size. Furthermore, detailed studies of microstructure evolution in Zircaloy-2 using unirradiated and irradiated materials suggested that the elevated content of alloying elements (iron, chromium and nickel) in the matrix would result in high nodular corrosion resistance [3–9].

Although most of the alloying elements exist as SPPs before irradiation, they dissolve into the Zircaloy-2 matrix during BWR irradiation, resulting in an increase of iron and nickel contents in the matrix. Since the dissolution rate could be affected by the specific surface area of the SPPs, i.e., their size, the original distribution of the SPPs would be a useful index for evaluating the corrosion behavior of Zircaloy-2 claddings in BWRs. Furthermore, recent studies have demonstrated that nodular corrosion resistant Zircaloy-2 with fine precipitates increased the uniform corrosion rate for long exposure times [1,3].

The objectives of this paper are to investigate the correlation of initial precipitate size with corrosion behavior of Zircaloy-2 claddings irradiated in commercial BWRs and to evaluate the preferable precipitate size for the current design of Zircaloy-2 tubes. Since recent data suggest that irradiation temperature may be important for the SPP behavior during irradiation, the effect of temperature on the dissolution of the particles is also discussed.

2. Experimental procedure

The maximum oxide thickness data of three types of Zircaloy-2 claddings, which were published elsewhere, were utilized in this study. They were from: 'Proving Test on Reliability for BWR Fuel Assemblies' (cladding A) [10], 'Verification Tests on BWR High Performance Fuel' (cladding B) [11,12] and 'Development of New Zr Alloys in a BWR' (cladding C) [13]. Since the Zircaloy-2 cladding

* Corresponding author. Tel.: +81-29 266 2131; fax: +81-29 266 2580; e-mail: shimada@nfd.co.jp.

PII S0022-3115(97)00124-4

tubes used for these programs differed from each other in fabrication process or heat treatment conditions, it was expected that their initial precipitate size distributions would also differ from one another. Cladding C was fabricated from ($\alpha + \beta$)-quenched tubeshells, or it is the current tubeshell heat treatment (TSHT) tube.

In order to correlate the initial particle sizes with corrosion behavior, the intermetallic particle size distributions in claddings, which were fabricated in the same way as claddings A, B and C, were studied using transmission electron microscopy (TEM). Those claddings are also designated as claddings A, B and C, hereafter. Energy dispersive X-ray spectroscopy (EDX) was also used on all particles to distinguish Zr(Fe, Cr)$_2$ and Zr$_2$(Fe, Ni) compounds. Diffraction patterns were also adopted to separate them when necessary. All of the TEM examinations were done on a Hitachi H-800 200 kV electron microscope equipped with a Horiba EMAX-2200 energy dispersive X-ray spectroscope. Tubing specimens were reduced to about 150 μm thickness by machining and then TEM discs were punched out having a diameter of 3 mm. The discs were electropolished in a 25% by volume perchloric acid in ethanol solution in a twinjet polisher at 15 V and 223 K. For the cladding A and B specimens, the TEM discs were prepared from the mid-wall of the tubing specimens, while for cladding C, they were prepared from an area near the outer surface and the observation area was about 5 μm from the surface. An imaging magnification of 100k was used to study the precipitates, and the particle sizes were calculated by an image analyzer. More than 200 precipitates were examined to get the initial particle size distribution histograms of the intermetallic compounds for each cladding type.

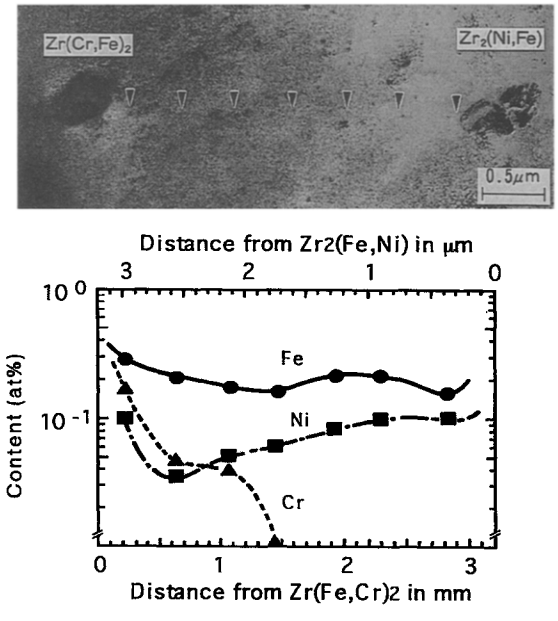

Fig. 1. Alloying element distributions in irradiated Zircaloy-2 exposed to a neutron fluence of 7×10^{25} n/m^2 ($E > 1$ MeV). The triangles in the TEM image denote analysis points corresponding to the plotted data.

Table 1
Irradiation conditions of cladding specimens D and E

Specimen	Neutron fluence ($\times 10^{25}$ n/m^2, $E > 1$ MeV)	Ramp test	
		peak power (kW/m)	hold time (h)
D	9.3	57	12
E	9.5	–	–

Since microstructure evolution of Zircaloy-2 when irradiated in a BWR is important for understanding the effect of precipitate size on corrosion behavior, the phenomenon is reviewed briefly here [8]. Most alloying elements, i.e., iron, chromium and nickel, exist as SPPs of intermetallic compounds. The major intermetallic compounds are hcp–Zr(Fe, Cr)$_2$ and bct–Zr$_2$(Fe, Ni). TEM examinations revealed that they behaved differently under BWR irradiation conditions. The hcp–Zr(Fe, Cr)$_2$ precipitates initiate a crystalline-to-amorphous transition from their periphery zones where distinct iron depletion occurs. In bct–Zr$_2$(Fe, Ni) precipitates, on the other hand, both iron and nickel dissolve into the matrix until finally they disappear. Due to this irradiation-induced redistribution, the contents of iron, chromium and nickel in the alloy matrix will be high as shown in Fig. 1, although they are too low in the matrix to be detected by a conventional EDX analysis for unirradiated materials [14]. However, the microstructure evolution caused by irradiation is temperature-dependent [2] and may be typical for BWR conditions. In order to confirm the temperature effect on the microstructure evolution of Zircaloy-2 in BWR conditions, two other types of cladding, D and E, were examined in terms of the microstructure evolution. Cladding D experienced a power-ramp test, i.e., a high temperature situation, after base irradiation, while cladding E experienced only base-irradiation. The irradiation conditions of the tube samples D and E are summarized in Table 1. Both D and E were zirconium-lined tubes.

Typical cladding temperatures at a peak linear heat rate (LHR) of 57 kW/m during the ramp test were calculated and tabulated in Table 2 as well as typical temperatures

Table 2
Calculated temperatures in cladding specimens D and E

Linear heat rate (kW/m)	Temperature (K)		
	inner surface	mid-wall	outer surface
20	598	584	570
57	650	611	572

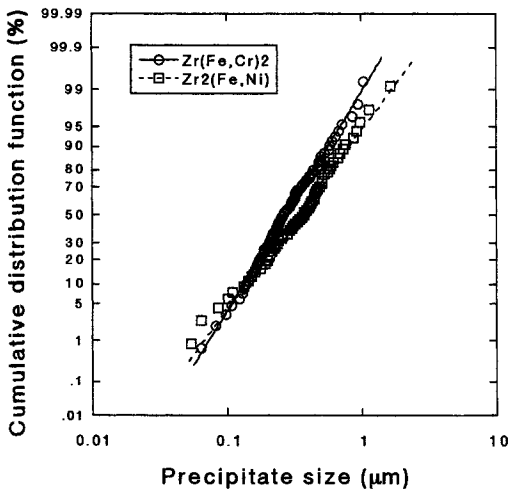

Fig. 2. Distribution of precipitates in cladding A.

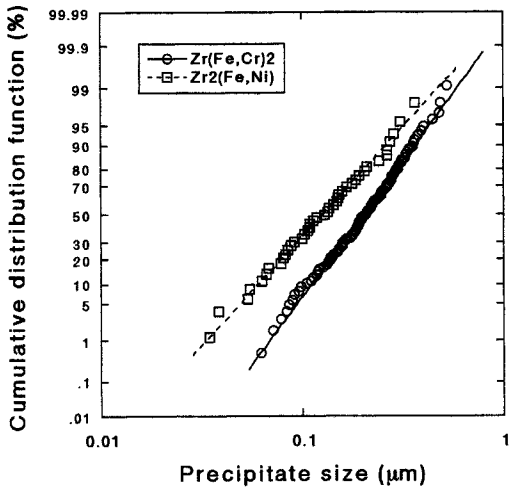

Fig. 3. Distribution of precipitates in cladding B.

during the base-irradiation with a LHR of 20 kW/m. In the ramp test, the tube was held at the peak power for 12 h. In order to examine the microstructure evolution of Zircaloy-2, the TEM specimens were prepared from the mid-wall of the tubing samples.

3. Results

An analysis of the initial size distribution of SPPs suggested that the distribution could be expressed by a log normal distribution just as noted by Huang et al. [15]. Therefore, the log normal distribution function was used to evaluate the particle size distribution of the three types of claddings. The cumulative distribution functions of the SPPs are plotted against their sizes for the claddings A, B and C in Figs. 2–4, respectively. The straight lines in the figures were calculated by a least-square fitting procedure. The fact that the data points could be represented by straight lines indicated, again, that the precipitate size distribution could be expressed by the log normal distribution. This result also indicates that the median precipitate size can be used as well as the mean size as an index of precipitate size [16]. Their mean and median precipitate sizes are tabulated in Table 3. The analysis showed that the median size was 0.85 time of the mean size.

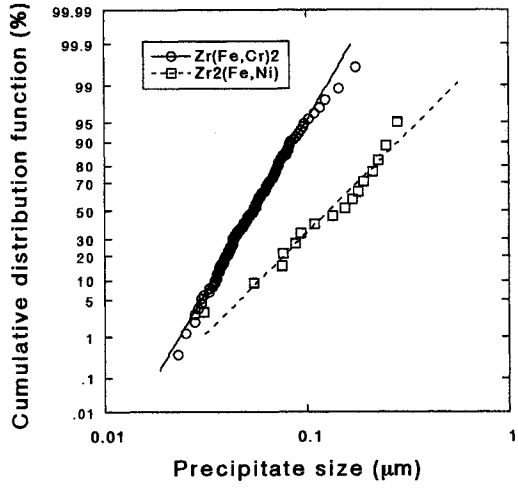

Fig. 4. Distribution of precipitates in cladding C.

The published data on the oxide thickness of claddings A, B and C were coupled with the mean precipitate sizes obtained by TEM/EDX observations to evaluate the effect

Table 3
Mean and median precipitate sizes of cladding A, B and C

Cladding	All precipitates		$Zr(Fe, Cr)_2$		$Zr_2(Fe, Ni)$	
	mean (μm)	median (μm)	mean (μm)	median (μm)	mean (μm)	median (μm)
A	0.364	0.301	0.324	0.264	0.418	0.373
B	0.201	0.187	0.224	0.206	0.147	0.130
C	0.069	0.056	0.058	0.054	0.153	0.152

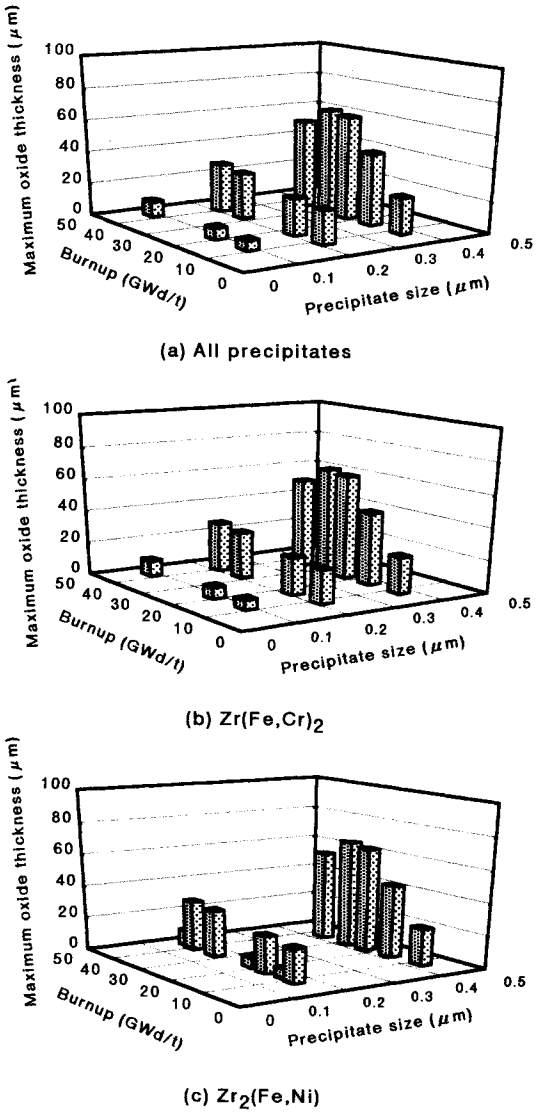

Fig. 5. Effects of mean precipitate sizes on corrosion behavior.

of initial precipitate size on corrosion behavior of Zircaloy-2 cladding tubes in BWRs. The results are summarized in Fig. 5.

When the microstructure of cladding D was examined by TEM and EDX, a new precipitate was found in addition to the usual $Zr(Fe, Cr)_2$ and $Zr_2(Fe, Ni)$ compounds. The new precipitates were located along the grain boundaries as shown in Fig. 6. The EDX analysis on the C_1 and C_2 precipitates in Fig. 6(a) showed they were composed of zirconium, iron and nickel. The TEM diffraction pattern of the precipitates suggested that the precipitates were zeta-phase particles with hcp crystalline structure, which has been found in Zircaloy post-irradiation annealed at 673 K [3,4,16,17]. The content differences of iron, chromium and nickel at the grain boundaries and in the matrix were

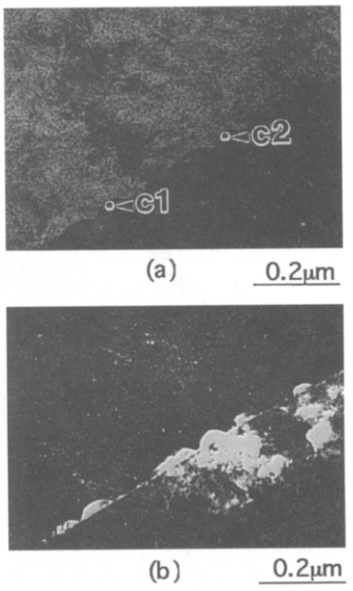

Fig. 6. Intergranular precipitates in the ramp-tested Zircaloy-2 cladding tube: (a) bright field image and (b) dark field image.

analyzed for specimens D and E. The results, as shown in Fig. 7, indicated that the boundaries of cladding D were enriched in iron, chromium and nickel relative to E. Furthermore, the EDX analysis revealed that iron also diffused back into the amorphous region of $Zr(Fe, Cr)_2$ compounds. These observations indicated that during the ramp test (611 K), iron, chromium and nickel in the matrix probably diffused back into the grain boundaries and the original SPPs.

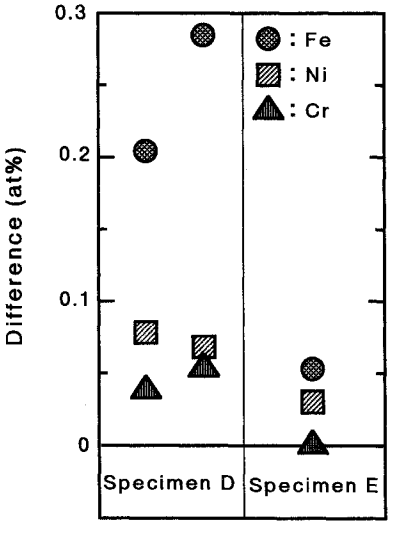

Fig. 7. Increase in alloying element contents near the grain boundaries for the ramp-tested Zircaloy-2 tube.

4. Discussion

Table 3 and Figs. 2–4 can be considered to show how the size and distribution of $Zr(Fe, Cr)_2$ and $Zr_2(Fe, Ni)$ compounds in Zircaloy-2 cladding tubes have changed historically. Cladding A, the oldest tube among them, has the largest SPP size. In particular the size of the $Zr_2(Fe, Ni)$ compound is substantial. The best fitting lines of cumulative distribution functions for both compounds show that their size distributions are similar, although their mean sizes are a little different.

As for cladding B, the mean particle sizes of both compounds are smaller than those of cladding A. This feature is more remarkable for the $Zr_2(Fe, Ni)$ compound. Therefore, the decrease in the particle size of the $Zr_2(Fe, Ni)$ compound may be a dominant factor for the change in corrosion behavior between claddings A and B.

The most notable features of the SPPs in cladding C is the very fine size of the $Zr(Fe, Cr)_2$ compound. Its mean size is about 25% of that in cladding B. Furthermore, the gradient of the best-fitted cumulative line indicates that the size distribution is controlled in a comparatively narrow range. By comparison, the $Zr_2(Fe, Ni)$ compound has almost the same mean size as cladding B. This suggests that the improved corrosion resistance of the current design cladding C is largely due to the existence of fine $Zr(Fe, Cr)_2$ precipitates.

The correlation between the corrosion behavior of these cladding tubes and the mean precipitate size summarized (Fig. 5) includes the mean size effect of $Zr(Fe, Cr)_2$, $Zr_2(Fe, Ni)$ and all precipitates. As mentioned above, both the $Zr(Fe, Cr)_2$ and $Zr_2(Fe, Ni)$ compounds seem to play a role in improving the corrosion behavior from claddings A–C, so that the mean size of all precipitates may be a good index for discussing the preferable precipitate size. Table 3 shows that the median precipitate size can be used as an index instead of the mean size. Fig. 5 indicates that the current cladding C has good corrosion behavior and the increase in its corrosion rate is very small even at high fluences. This result gives the impression that an even finer precipitate size should result in better corrosion behavior. However, a recent report [15] suggested that some lower limit exists in the particle size from the engineering viewpoint of fabricating cladding tubes. As is well known, β- or (α + β)-quench is necessary to get the fine precipitate size in Zircaloy-2. But an annealing treatment in the α-phase region is needed after the quench process to fully recrystallize the materials, which means that growth of precipitates is inevitable during the heat treatment. This report showed that the heat treatment which caused the growth of precipitates to a mean size of about 0.04 μm did not produce the ordinary matrix structure observed in Zircaloy-2 cladding tubes. The results indicated that a mean precipitate size of more than 0.05 μm would be the limit for actual cladding tube materials for BWRs. Then, the particle size of about 0.07 μm achieved in the current cladding C should be in the most preferable range for BWR cladding tubes. The report [15] also suggested that when corrosion behavior of Zircaloy-2 with fine precipitate size is studied, in addition to the effect of precipitate size, careful attention should be paid to the effects from other microstructures, such as β-phase and localized precipitate distribution.

Although irradiation-induced dissolution of the SPPs predominates under BWR conditions, this study showed that, at a temperature of 611 K, re-precipitation of zeta-phase particles would take place. Considering the fact that the re-precipitation of zeta-phase hardly occurred at 589 K [3], the re-precipitation must become active at more than about 600 K. This result and the microstructure evolution of Zircaloy-4 for pressurized water reactor (PWR) conditions [18] demonstrate that irradiation induced dissolution of $Zr(Fe, Cr)_2$ compounds and re-precipitation of the zeta-phase particles might occur at the same time in PWRs.

5. Conclusion

The effects of original precipitate sizes and distributions on the corrosion behavior of Zircaloy-2 cladding tubes in BWRs were examined. The TEM/EDX observations revealed that the decrease in initial precipitate sizes of both $Zr(Fe, Cr)_2$ and $Zr_2(Fe, Ni)$ contributed to the increase in corrosion resistance of the tubes. Especially, the very fine size of the $Zr(Fe, Cr)_2$ compound in current Zircaloy-2 cladding played an important role in getting high corrosion resistance under BWR conditions. However, it was pointed out that the fabrication process of cladding tubes imposed a minimum precipitate size on the tubes and the size would be about 0.06 μm. A comprehensive evaluation of the preferable mean precipitate size for corrosion behavior suggested that the size of about 0.07 μm, that of current cladding tube, was in the most suitable range.

The TEM/EDX examinations of Zircaloy-2 tubes which had experienced a power ramp test, i.e., which were exposed to a temperature of 611 K for 12 h, revealed that zeta-phase particles re-precipitated at grain boundaries and iron diffused back into the $Zr(Fe, Cr)_2$ compounds in the cladding. This observation indicated that both dissolution and re-precipitation occurred near 611 K and that microstructure evolution was sensitive to the temperatures experienced by cladding tubes in light water reactors.

References

[1] F. Garzarolli, R. Schumann, E. Steinberg, ASTM STP 1245 (1994) 709.
[2] P. Rudling, M.M. Lindback, B. Lethinen, H.O. Andren, K. Stiller, ASTM STP 1245 (1994) 599.
[3] B. Cheng, R.M. Kruger, R.B. Adamson, ASTM STP 1245 (1994) 400.

[4] R.M. Kruger, R.B. Adamson, S.S. Brenner, J. Nucl. Mater. 189 (1992) 193.
[5] Y. Etoh, K. Kikuchi, T. Yasuda, S. Koizumi, M. Oishi, Proc. Int. Topical Meeting on LWR Fuel Performance, Avignon, Apr. 21–24, 1991, p. 691.
[6] Y. Etoh, S. Shimada, K. Kikuchi, K. Kawai, J. Nucl. Sci. Tech. 29 (1992) 1173.
[7] Y. Etoh, S. Shimada, J. Nucl. Sci. Tech. 29 (1992) 358.
[8] Y. Etoh, S. Shimada, J. Nucl. Mater. 200 (1993) 59.
[9] W.J.S. Yang, F.P. Tucker, B. Cheng, R.B. Adamson, J. Nucl. Mater. 138 (1986) 185.
[10] Y. Mishima, J. At. Energ. Soc. Jpn 29 (1987) 90.
[11] K. Ogata, Y. Etoh, K. Ito, K. Une, Y. Iseki, T. Nomata, M. Irube, M. Futakuchi, Fall Meeting of the Atomic Society of Japan, (1994) J30.
[12] S. Muto, Y. Hayashi, T. Yasuda, T. Koyama, K. Koizumi, Proc. Int. Topical Meeting on LWR Fuel Performance, American Nuclear Society, West Palm Beach, FL, Apr. 17–21, 1994, p. 71.
[13] Y. Etoh, S. Shimada, T. Yasuda, T. Ikeda, R.B. Adamson, J.F. Chen, Y. Ishii, K. Takei, ASTM STP 1296 (1996) 825.
[14] D. Charquet, R. Hahn, E. Ortlieb, J.P. Gros, J.F. Wadier, ASTM STP 1023 (1989) 405.
[15] P.Y. Huang, S.T. Mahmood, R.B. Adamson, ASTM STP 1295 (1996) 726.
[16] M. Griffiths, R.W. Gilbert, G.J.C. Carpenter, J. Nucl. Mater. 150 (1987) 53.
[17] W.J.S. Yang, EPRI NP-5591 (1988).
[18] D. Gilbon, C. Simonot, ASTM STP 1245 (1994) 521.